

# Evaluating Liquefaction Susceptibility Through HVSR and MASW Methods: A Case Study in Mamuju, West Sulawesi, Indonesia

Rudarsko-geološko-naftni zbornik (The Mining-Geology-Petroleum Engineering Bulletin) DOI: 10.17794/rgn.2025.5.1

Original scientific paper



Andri Moh. Wahyu Laode¹ (□) □, Muh. Altin Massinai¹\* (□) □, Muhammad Fawzy Ismullah Massinai¹,² (□) □, Erfan Syamsuddin¹ (□) □

- Department of Geophysics, Faculty of Mathematics and Natural Science, Hasanuddin University, South Sulawesi 90245, Indonesia.
- <sup>2</sup> Geology Program, Department of Earth Sciences and Environment, Faculty of Science and Technology, Universiti Kebangsaan Malaysia, 43600 UKM Bangi, Selangor Darul Ehsan, Malaysia.

#### **Abstract**

The 2021 Mamuju earthquake (Mw 6.2) highlighted the region's high vulnerability to liquefaction due to its proximity to active tectonic zones, as well as the presence of Holocene alluvial deposits, unconsolidated sedimentary formations, and water-saturated soils, all of which contribute to high susceptibility to seismic shaking. This research assesses the liquefaction potential of the Mamuju area using an integrated approach that combines the Horizontal-to-Vertical Spectral Ratio (HVSR) and Multichannel Analysis of Surface Waves (MASW) methods. This study investigates an inverse correlation between Vs30 and the seismic vulnerability index ( $K_g$ ), where lower  $V_{s30}$  values correspond to higher Kg values, indicating increased liquefaction susceptibility. The HVSR analysis shows that the dominant frequency ( $f_0$ ) ranges from 0.4 to 11 Hz, while the amplification factor ( $f_0$ ) varies between 1.1 and 11. The results indicate that coastal zones with thick alluvial deposits exhibit the lowest  $f_0$  values (<2.5 Hz), which correlate with  $V_{s30}$  < 175 m/s and  $K_g$  > 10, suggesting a higher likelihood of liquefaction. Conversely, areas underlain by the Mamuju Formation and Adang Volcanics, characterized by higher  $V_{s30}$  (>175 m/s),  $f_0$  (>10 Hz), and  $f_0$  (<10), show lower susceptibility. These findings contribute to developing a detailed microzonation map for liquefaction risk, which is essential for improved urban planning and disaster mitigation in Mamuju. This study demonstrates that integrating HVSR and MASW methods is an effective approach to characterizing soil properties and enhancing liquefaction risk assessment in seismically active regions.

#### **Keywords:**

liquefaction, HVSR, MASW, Seismic Vulnerability Index, shear wave velocity, Mamuju earthquake

#### 1. Introduction

The Mamuju region is located in a highly earthquakeactive area of West Sulawesi. Based on the research of (Hanifa et al., 2022; Meilano et al., 2023), such conditions were due to the position near the convergence of three tectonic plates, which are the Eurasian Plate, the Indo-Australian Plate, and the Pacific Plate (Sompotan. 2012; Supendi et al., 2021). The movement of these plates exerts additional stress on the tectonic setting of Sulawesi, contributing to complex fault dynamics, increasing strain accumulation, and enhancing the likelihood of fault rupture, thereby affecting the seismic vulnerability of the Mamuju region. The movement of these plates may trigger subduction zones and active faults that can potentially produce high-magnitude earthquakes (Rosid et al., 2022). As a result of this high tectonic activity, the Mamuju region frequently experiences significant and destructive earthquakes (Meilano et al., 2023).

\* Corresponding author: Muh. Altin Massinai e-mail address: altin@science.unhas.ac.id
Received: 12 January 2025. Accepted: 1 April 2025.

Available online: 21 October 2025

One of the destructive impacts of earthquakes is the phenomenon of soil liquefaction. Soil liquefaction is a phenomenon in which saturated, loosely packed soil temporarily loses its strength and stiffness due to a sudden increase in pore water pressure induced by cyclic loading from earthquake shaking, causing it to behave like a liquid (Sukkarak et al., 2021; Tabrizi-Zarringhabaei et al., 2019; Zhou et al., 2020). This condition can result in severe damage to infrastructure and buildings, such as ground subsidence, lateral spreading, and structural collapse (Chaloulos et al., 2020). Therefore, identifying areas vulnerable to liquefaction is crucial for earthquake disaster risk mitigation efforts (Bao et al., 2019; Mahmoud et al., 2020).

The 2021 Mamuju earthquake (Mw 6.2) underscored the need for a detailed assessment of soil vulnerability to liquefaction in the region (Hanifa et al., 2022; Hossain et al., 2020). Indications such as ground settlement and increased pore water pressure were reported in several areas (see Figure 2A-E), highlighting the importance of evaluating liquefaction susceptibility (BMKG, 2021). This study aims to analyze soil vulnerability and map liquefaction risks in Mamuju using the HVSR (Horizon-

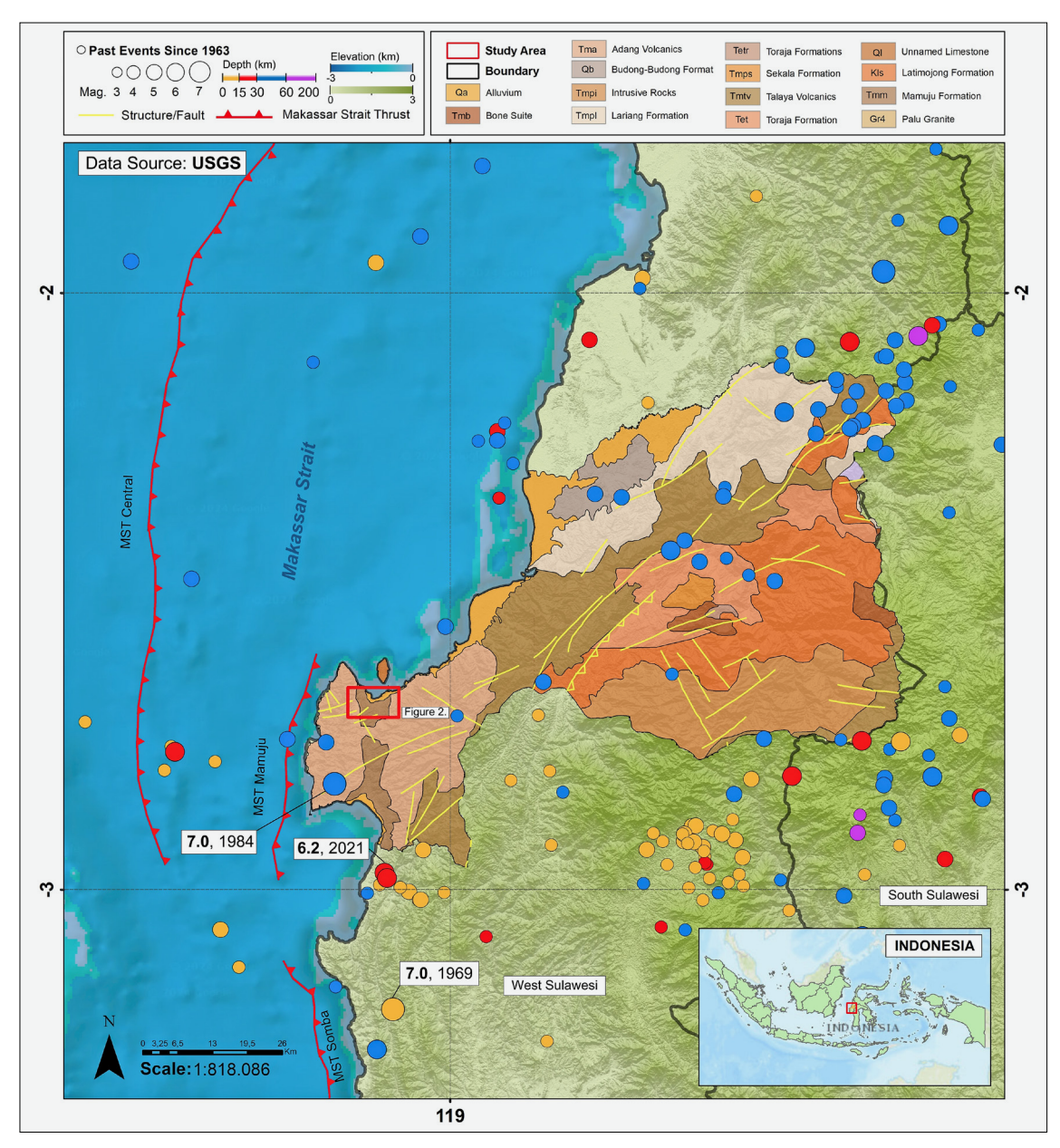
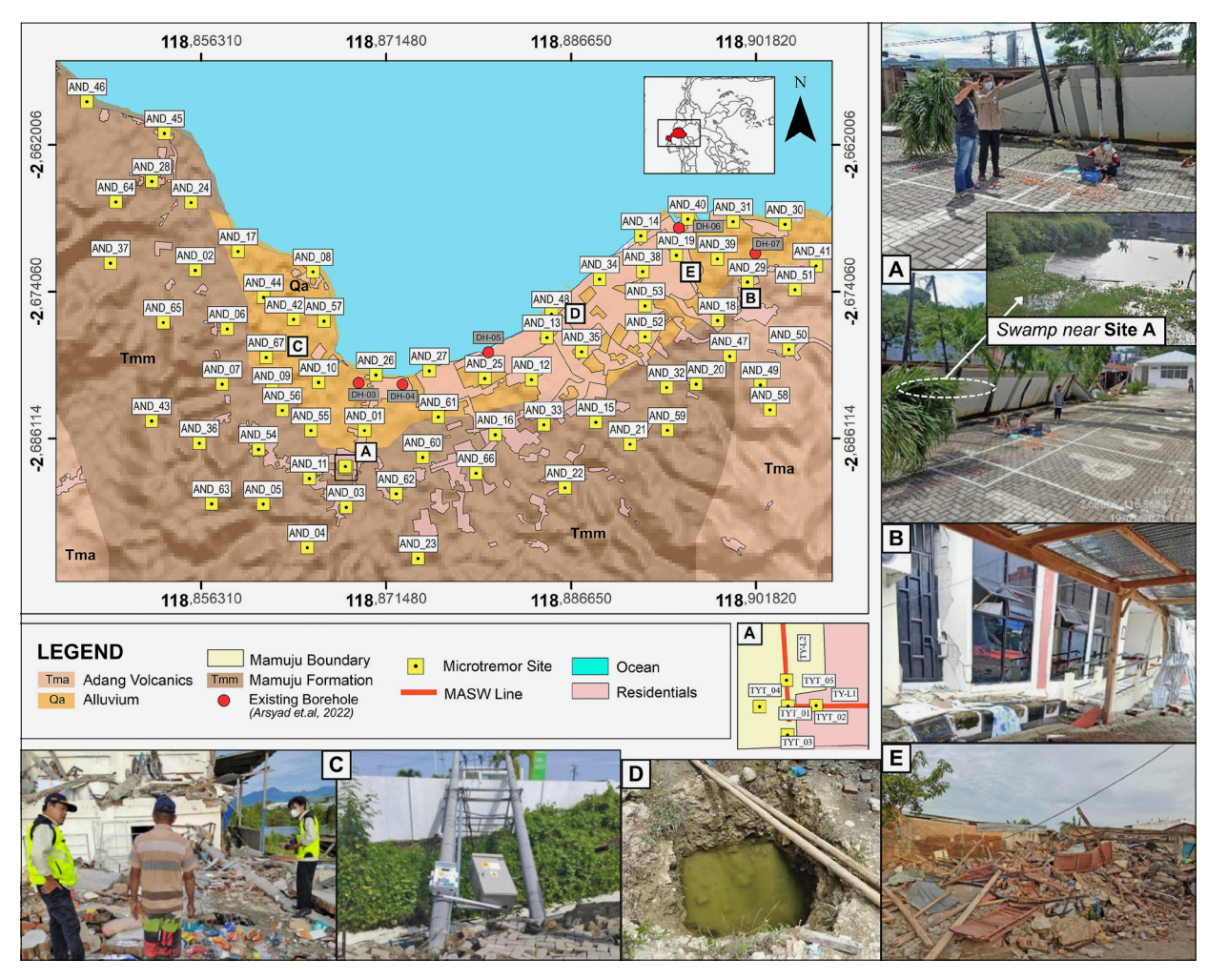


Figure 1. The geological formations and seismic activity in the study area. On January 15, 2021, a Mw 6.2 earthquake occurred near the active Makassar Strait Thrust (MST) system. Significant historical events in the region include the Mw 7.0 earthquake in 1969 and the Mw 7.0 earthquake in 1984. The colored circles represent seismic activity recorded from 1963 to 2024, based on data from the United States Geological Survey (USGS) Catalog. The colors of the circles indicate differences in earthquake depth, while the circle size represents the earthquake magnitude.

tal to Vertical Spectral Ratio) and MASW (Multichannel Analysis of Surface Waves) methods (Quintero et al., 2023; Roy et al., 2022). The MASW method utilizes an active seismic wave source and records the propagation of surface waves to obtain shear wave velocity  $(V_s)$  profiles (Alan et al., 2019; Liu et al., 2020; Mohammed et al., 2020). In contrast, the HVSR method captures ambient vibrations at the study site (Nguyen-Tien et al., 2022; Piña-flores et al., 2020; Sedaghati et al., 2018) to determine natural frequency, ground amplification, and the seismic vulnerability index (Akkaya, 2020; Yaghmaei-Sabegh & Rupakhety, 2020), which are key

indicators in assessing liquefaction potential (Kang et al., 2020). Integrating these two methods provides a more comprehensive understanding of soil properties and seismic response, essential for accurate liquefaction risk assessments (Alkan & Akkaya, 2023; Uyanık, 2020).

Previous studies have demonstrated the effectiveness of combining MASW and HVSR in assessing soil vulnerability and liquefaction risk in various regions (Chiaradonna et al., 2022; Kang et al., 2021; Mahajan et al., 2012; Mase et al., 2018; Pamuk et al., 2018; Shelley et al., 2015; Sundararajan & Seshunarayana, 2011; Syamsuddin et al., 2024). These studies highlight



**Figure 2.** HVSR and MASW survey locations and geological formations of the study area. **A–D** indicate locations affected by the 2021 Mamuju earthquake, showing damage features such as sand boils, ground subsidence, collapsed buildings, and the emergence of water from previously dry holes (**BMKG**, 2021).

the ability of MASW to delineate shear wave velocity profiles, while HVSR provides insight into site resonance frequency, amplification factors, and seismic vulnerability index, making it possible to identify subsurface conditions that contribute to the potential for liquefaction. However, most of these studies have been conducted in regions with well-documented seismic histories, whereas limited research has explored the applicability of these methods in Sulawesi, particularly in Mamuju, where recent earthquakes have caused significant damage.

Existing seismic studies in Mamuju have primarily focused on macroseismic observations and general geological assessments (**Supendi et al., 2021**), lacking detailed microzonation efforts that integrate geophysical methods to quantitatively assess liquefaction susceptibility. Furthermore, while MASW and HVSR have been used separately in other earthquake-prone regions, their combined application to analyze liquefaction susceptibility in Mamuju remains unexplored. This study fills this gap by integrating MASW and HVSR techniques to obtain high-resolution  $V_s$  profiles, seismic vulnerability

index, and site amplification characteristics. The findings contribute to refining seismic hazard models, enhancing spatial planning strategies, and improving earthquake disaster mitigation efforts, particularly in Mamuju, a region with high seismic activity.

## 2. Tectonic Activity and Geological Setting

Due to its position at the triple junction of the Australian Plate, Sunda Plate, and Philippine Sea Plate, Sulawesi Island in eastern Indonesia experiences the relative displacement of at least four microblocks through active faulting (Simons et al., 2007). In West Sulawesi, the eastern boundary of the Sunda Plate is marked by the Makassar Block. The relative movement between the Makassar Block and the Sunda Plate is accommodated by the Makassar Strait Thrust (MST), which is divided into the Somba, Mamuju (MSTM), Central (MSTC), and Northern (MSTN) segments (Meilano et al., 2023). Although the slip rate of the MST is about one-quarter that of the Palu-Koro Fault, the MST remains a significant earthquake threat to communities along the western

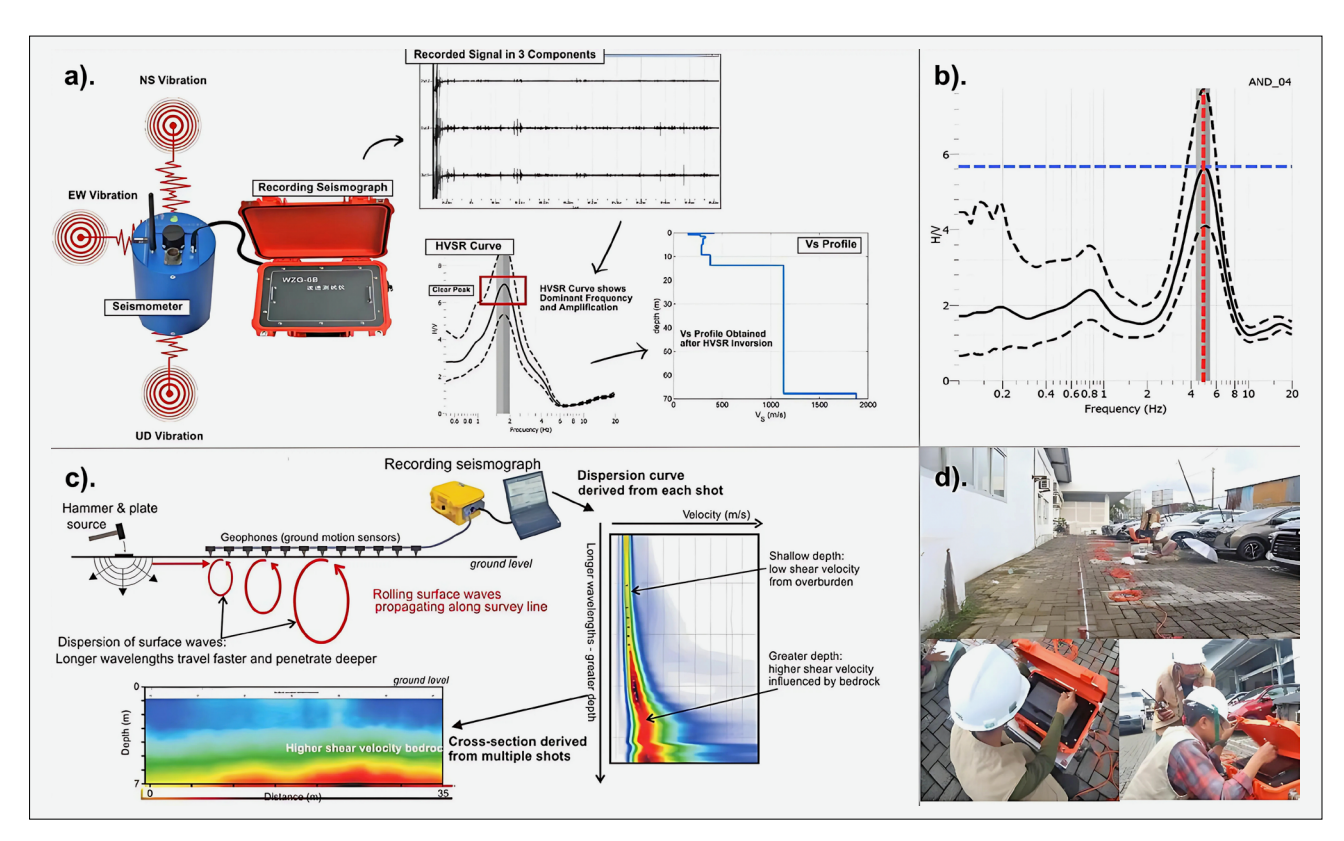


Figure 3. a) HVSR measurement procedure. b) Example of HVSR curve at station AND\_04 (black line), maximum and minimum standard deviation (dashed black line). The dashed red vertical line shows the dominant frequency processed through GEOPSY software. The dashed blue horizontal line shows the maximum amplitude of the dominant frequency.

c) MASW measurement procedure (TERRADAT, 2024). d) HVSR and MASW data acquisition at the research site.

Sulawesi coast, especially in Mamuju Regency (Supendi et al., 2021). Notable earthquakes along the MST (as seen in Figure 1) include the 1969 Majene earthquake (Mw 7.0), the 1984 Mamuju earthquake (Mw 7.0), and the 6.2 Mw earthquake on January 15, 2021. The 2021 earthquake occurred near the active MST system, following a Mw 5.9 earthquake 12 hours before the main shock (Meilano et al., 2023; Supendi et al., 2021).

The Mamuju region consists of sedimentary, metamorphic, volcanic, and intrusive rock formations ranging from the Mesozoic to the Quaternary (see Figure 1). The Latimojong Formation, the oldest unit, comprises metamorphic rocks such as quartzite, phyllite, and marble (White et al., 2017). Overlying it, the Toraja, Sekala, and Lariang Formations are composed of sandstone, shale, marl, and carbonate-rich deposits, representing marine to transitional depositional settings (Ardianto et al., 2024). Volcanic activity is recorded in the Talaya and Adang Volcanics, which consist of volcanic breccia, lava flows, tuff, and basaltic rocks, while Quaternary deposits, including the Budong-Budong Formation and alluvium, cover coastal and riverine areas (Perdana & Amijaya, 2011; White et al., 2017). The structural geology of the region is dominated by faults trending northeast-southwest and northwest-southeast, which have resulted in faulting, folding, and uplift. The highlands, primarily composed of metamorphic and volcanic rocks,

contrast with the lowlands, which are covered by unconsolidated Quaternary sediments that are more susceptible to seismic amplification and liquefaction (Rosianna et al., 2020).

A) The research site indicated to have experienced liquefaction, marked by sand boils on the pavement blocks and collapsed walls, with a swamp located near site A (BMKG, 2021). B) Collapsed building accompanied by ground subsidence at the Mamunyu Subdistrict Office, Mamuju (BMKG, 2021). C) Ground subsidence and collapsed buildings in a residential area. D) Emergence of water in previously dry holes due to increased pore water pressure (BMKG, 2021). E) Collapsed buildings in a residential area near the Mamuju port (BMKG, 2021).

The study area comprises three geological formations: Alluvium, Mamuju Formation, and Adang Volcanics (as shown in **Figure 2**). The Alluvium Formation consists of loose sediment deposits commonly found in lowland areas near the coast and along rivers. These water-saturated alluvial layers are prone to liquefaction because they are highly susceptible to deformation due to earthquake shaking. The Mamuju Formation is composed of marl, calcareous sandstone, coral limestone, and tuffaceous sandstone, with local occurrences of conglomerate and claystone. This formation represents a shallow marine depositional environment, characterized by carbonate sedimentation interbedded with volcani-

clastic deposits (Perdana & Amijaya, 2011; White et al., 2017). The presence of poorly consolidated marl and tuffaceous sandstone indicates weak lithification, making the formation more susceptible to deformation under seismic loading (Rosianna et al., 2023). The Adang Volcanics consist of various volcanic rocks, primarily phonolitic leucite, containing minerals like leucite, Kfeldspar, plagioclase, pyroxene, and small amounts of opaque minerals (Shaban et al., 2016). These rocks tend to undergo moderate to strong weathering (Ritonga et al., 2021). Overall, the Mamuju region and its surroundings are characterized by numerous geological formations dominated by loose sediment deposits, both in lowland areas and hills. The predominance of loose sediments increases the region's vulnerability to the destructive impacts of earthquakes (Rosianna et al., 2020; Zaidani et al., 2023).

#### 2. Data and Methods

#### 2.1. Data

The data used in this study consist of measurements from 72 microtremor sites and 2 MASW lines spread across Mamuju, West Sulawesi (see Figure 2). MASW data acquisition was conducted with a sampling rate of 0.5 ms and a sampling frequency of 2000 Hz, with a recording duration of 1.024 s. The survey utilized 24 geophones with a natural frequency of 4.5 Hz, arranged in a straight line, with a near-offset of 5 meters and a spacing of 1 meter between geophones. A sledgehammer was used as an active source. The roll-along configuration was employed to obtain 2D data. For line 1, the sourcereceiver was shifted 2 meters with a total of 12 shots, while for line 2, the source receiver was moved 1 meter with a total of 13 shots. The difference in geometry between the two profiles was due to field conditions that prevented the use of the same geometry. The documentation of microtremor HVSR and MASW acquisition is presented in Figure 3d.

Microtremor measurements were conducted for durations of 20-60 minutes with a sampling frequency of 100 Hz and a sampling rate of 0.01 s using a Digital Portable Seismograph type TDL-303S and a seismometer type DS-4A. The recorded data consisted of three components of the seismogram: the horizontal components (North-South and East-West) and the vertical component (Up-Down) (Mihaylov et al., 2019). The recorded data were then processed to obtain HVSR using the following Equation 1 (Khalili & Mirzakurdeh, 2019; Ma et al., 2019):

$$HVSR = \sqrt{\frac{H_{NS}^2 + H_{EW}^2}{V^2}}$$
 (1)

Where:

HVSR – horizontal to vertical spectral ratio,

- amplitude spectrum of the north-south horizontal component,

- amplitude spectrum of the east-west hori-

- amplitude spectrum of the vertical compo-

#### 2.2. Method

The Horizontal-to-Vertical Spectral Ratio (HVSR) method is a passive geophysical technique used to evaluate the dynamic properties of soil and local site effects (Chávez-García & Raptakis, 2017; Maghami et al., 2021; Maklad et al., 2020). The fundamental principle of HVSR involves recording ambient vibrations using a three-component seismometer (Bignardi, 2017; Gupta et al., 2021). These vibrations originate from various natural and anthropogenic sources, such as wind, ocean waves, and human activities (Ahn et al., 2021; Yang et al., 2019). The recorded data are then analyzed to produce the HVSR curve (see Figure 3b), which displays the spectral amplitude ratio of the horizontal to vertical components as a function of frequency (Fat-Helbary et al., 2019; Molnar et al., 2022). A reliable HVSR curve must meet the criteria established by SESAME (2004). These criteria include the stability of the HVSR curve across different time windows, the presence of a clear peak (as shown in Figure 3b), a low standard deviation within one octave of the fundamental frequency (fo), and consistency in amplitude and shape between the three components. Data that fulfill these conditions are considered reliable and suitable for further interpretation. The HVSR measurement procedure can be seen in Figure 3a. Peaks in the HVSR curve indicate the dominant frequency of the soil layers (Moon et al., 2019), which is directly correlated with the thickness and shear wave velocity of the sediment layers above the bedrock (**Perez, 2024**). The value of the dominant frequency  $(f_0)$ for a region can be expressed by the following Equation 2 (Nakamura, 2000):

$$f_0 = \frac{V_s}{4H} \tag{2}$$

Where:

fo – dominant frequency (Hz),

 $V_s$  – shear wave velocity (m/s), H – thickness of the sediment layer (m).

Soil vulnerability to liquefaction is assessed using the seismic vulnerability index  $(K_a)$  derived from HVSR.  $K_a$ identifies the susceptibility of a soil layer to deformation due to earthquakes (**Pamuk et al., 2018**). High  $K_{\alpha}$  values indicate that an area is prone to seismic effects (Livaoğlu et al., 2019), especially in soils with soft sedimentary rock lithology, such as coastal zones dominated by Alluvium formations (Putti & Satyam, 2020). These loose sediments, composed of sand, clay, and silt, have low cohesion and high water content, making them more susceptible to liquefaction during strong ground shaking (Sana & Nath, 2016). Liquefaction occurs when watersaturated, loose granular soils lose their shear strength due to increased pore water pressure during seismic shaking, resulting in fluid-like behaviour of the ground (Hanindya et al., 2023; Kusmanto et al., 2024). This phenomenon may lead to ground subsidence, lateral spreading, and structural damage (Kang et al., 2020). The  $K_a$  index is particularly useful in identifying highrisk zones where seismic and liquefaction hazards are not immediately apparent from surface observations. A value of  $K_a > 10$  suggests potential deformation, including liquefaction, whereas  $K_a < 10$  indicates more compact and stable soils that are less prone to seismic stressinduced failure (Akkava, 2020; Kang et al., 2021). Surface soil characteristics can be analyzed through the dominant frequency obtained from HVSR (Chen et al., 2020; Rong et al., 2020). Ground motion at a location is usually associated with a dynamic strain induced by seismic vibrations (Trifunac, 2016) and is often evaluated using the seismic vulnerability index  $(K_{\alpha})$  through the following Equation 3 (Susilo et al., 2023):

$$K_g = \frac{A_0^2}{f_0} \tag{3}$$

Where:

 $A_0$  – amplification,

fo - dominant frequency (Hz),

 $K_{\sigma}$  – seismic vulnerability index.

In addition to the  $K_g$  value,  $V_{s30}$  (the average shear wave velocity at a depth of 30 meters) is derived from V profiles at each microtremor site through HVSR inversion (Sivaram et al., 2018). Soil layers with low  $V_s$  values generally indicate soft or loose soils (Najaftomarei et al., 2020), which are more vulnerable to changes in characteristics during strong vibrations (Senkaya et al., **2019**). In contrast, high  $V_s$  values indicate denser and more stable soils, with a lower risk of structural changes during shaking (Salleh et al., 2021). To further analyze subsurface characteristics, spatial maps of dominant frequency (fo), seismic vulnerability index  $(K_g)$ , and  $V_{s30}$ were generated using interpolation techniques. Specifically, the Inverse Distance Weighting (IDW) method was applied to estimate values at unsampled locations by computing a weighted average of nearby measured points, where weights are inversely proportional to the distance (Ghione et al., 2023; Odom & Doctor, 2023). This method was chosen for its effectiveness in capturing local variations in geophysical parameters while maintaining computational efficiency (Qadri et al., **2015**). In this study,  $V_{\alpha}$  for shallow layers were also obtained using MASW surveys conducted at locations previously identified as areas susceptible to liquefaction. The Multichannel Analysis of Surface Waves (MASW) utilizes surface wave analysis (Rayleigh waves) to derive shear wave velocity  $(V_s)$  profiles in the soil layers (Abudeif et al., 2019; Liu et al., 2020). The acquired MASW data were processed using the Geopsy software, where dispersion curves were extracted and inverted using the Neighborhood Algorithm (NA) to derive the 1D shear wave velocity  $(V_s)$  profiles. These 1D profiles were then interpolated to construct a 2D  $V_s$  model to characterize subsurface conditions. The interpolation method used was kriging, which provides a statistically optimal estimation of  $V_s$  distribution by considering spatial correlations between data points, thereby ensuring a smooth and continuous representation of subsurface velocity variations (Ismail et al., 2014). The reliability of the  $V_s$  profile is evaluated based on the fit between the theoretical and experimental dispersion curves (Foti et al., 2015). The *misfit* value is a parameter that quantifies the discrepancy between experimental and theoretical dispersion curves and is calculated using the following Equation 4 (Wathelet et al., 2004):

$$misfit = \sqrt{\sum_{i=0}^{n_F} \frac{(x_{di} - x_{ci})^2}{\sigma_i^2 n_F}}$$
 (4)

Where

 $x_{di}$  – experimental Rayleigh wave phase velocity (m/s),

 $x_{ci}$  – theoretical Rayleigh wave phase velocity (m/s),

 $n_F$  – number of frequency samples,

 $\sigma_i$  – the uncertainty of the frequency samples considered.

The lower the value of misfit, the better the match between the experimental and theoretical dispersion curve, indicating a more reliable  $V_s$  model (Griffiths et al., 2016). The MASW procedure is shown in Figure 3c.

## 3. Results

In evaluating the liquefaction potential in Mamuju, West Sulawesi, the ambient noise recorded at 72 sites met the HVSR curve criteria in accordance with **SESA-ME (2004)**. The results are shown in **Table 1**.

# 3.1. Dominant Frequency

The dominant frequency, which refers to the fundamental resonance frequency of a site, is a crucial parameter in assessing site response to seismic activity (Syamsuddin et al., 2024). The frequency is inversely related to the thickness of the soil layer above bedrock, lower frequencies suggest deeper unconsolidated layers, while higher frequencies correspond to shallower layers (Kang et al., 2021; Pamuk et al., 2018). The results of the dominant frequency obtained at each site can be seen in Figure 4.

The dominant frequency values obtained at each site range from 0.4 to 12.6 Hz. Sites with low dominant frequencies (<2.5 Hz) are predominantly located along the coastline, indicating thick sediment layers with an alluvial rock formation. Medium dominant frequencies (2.5 – 10 Hz) are mainly found in areas with higher elevations, although some are also near the coastline. Sites

Table 1. HVSR Results at each station in Mamuju, West Sulawesi

ID	Longitude	Latitude	f <sub>0</sub> (Hz)	$\mathbf{A_0}$	$K_{\sigma}$	$V_{s3\theta}$ (m/s)
AND_01	707861	9703015	1.7	7.0	16.8	178
AND 02	706320	9704472	0.5	3.5	14.4	128
AND 03 AND 04	707694 707338	9702319 9701954	1.0	3.3	6.7	125 187
AND 05	706937	9702350	2.4	2.3	1.3	205
AND 06	706611	9703939	1.2	2.4	2.7	164
AND 07	706564	9703439	4.6	1.9	0.5	251
AND_08	707394	9704458	0.5	2.7	8.0	143
AND 09	707020	9703381	11.0	5.0	1.3	274
AND 10 AND 11	707442 707358	9703453 9702582	0.6	4.8	22.9	126
AND 12	709386	9702382	2.3	2.6	2.6	180 187
AND 13	709526	9703857	1.2	3.3	5.4	197
AND 14	710384	9704778	0.9	2.5	4.1	159
AND 15	709972	9703088	1.6	5.0	9.6	178
AND 16	709054	9702977	1.0	5.5	17.9	174
AND 17 AND 18	706710 711084	9704642 9704010	2.9 0.7	6.6 3.5	9.1	164 133
AND 19	710708	9704602	0.8	7.7	44.9	164
AND 20	710708	9703433	4.7	1.8	0.4	214
AND 21	710282	9702888	5.6	2.0	0.4	282
AND 22	709688	9702492	1.4	3.3	4.7	179
AND 23	708347	9701854	3.0	2.1	0.9	245
AND 24 AND 25	706283 708959	9705088 9703487	5.5 1.0	4.5	2.2 5.0	222 180
AND 26	707966	9703487	0.9	4.9	15.6	122
AND 27	707500	9703556	1.2	5.2	13.8	177
AND 28	705926	9705280	4.9	3.1	1.2	220
AND 29	711357	9704358	0.4	3.9	21.8	142
AND 30	711700	9704880	1.6	5.4	10.8	195
AND 31 AND 32	711226 710618	9704906 9703401	1.3	4.8	10.7	166 129
AND 32 AND 33	709496	9703066	0.4	2.6	9.4 5.6	149
AND 34	710007	9704387	6.7	3.7	1.2	268
AND 35	709843	9703728	3.9	2.9	1.3	155
AND 36	706354	9702903	0.8	6.1	27.3	155
AND 37	705546	9704538	2.7	2.7	1.6	196
AND 38	710400	9704454	3.8	3.7	2.1	185 199
AND 39 AND 40	711083 710812	9704569 9704931	1.3	2.7	2.1 3.4	146
AND 41	711983	9704505	0.8	3.1	7.3	170
AND 42	707216	9704024	0.5	6.1	44.3	138
AND 43	705920	9703106	10.8	3.1	0.5	243
AND 44	706941	9704225	1.0	2.8	4.9	142
AND 45	706040	9705716	0.4	4.4	28.1	138
AND 46 AND 47	705334 711194	9706005 9703685	8.3	3.2	3.5 1.0	157 312
AND 48	709567	9704070	0.8	5.6	24.3	140
AND 49	711473	9703421	6.7	3.5	1.1	275
AND 50	711732	9703745	2.4	3.7	3.4	209
AND 51	711789	9704287	2.3	3.2	2.7	243
AND 52 AND 53	710421 710421	9703864 9704144	3.5 0.8	3.2 2.8	1.8 5.6	282 136
AND 54	706894	9702847	1.7	7.0	16.8	147
AND 55	707373	9703016	0.5	3.6	15.6	149
AND 56	707111	9703199	2.4	2.3	1.3	137
AND 57	707493	9704010	0.7	3.5	10.0	114
AND 58	711560	9703196	4.7	1.8	0.4	228
AND 59 AND 60	710626 708391	9703013 9702772	4.3 3.2	1.1	0.2	165 231
AND 61	708535	9703139	0.9	4.9	16.5	151
AND 62	708355	9702440	0.7	1.5	2.2	125
AND 63	706465	9702352	3.0	2.0	0.8	154
AND 64	705596	9705093	3.4	2.0	0.7	204
AND 65	706028	9703999	9.9	3.7	0.8	291
AND 66 AND 67	708879 706966	9702626 9703681	3.7	3.3	1.8 127.8	231
TYT 01	707687	9702681	0.8	1.7	2.2	114
TYT 02	707677	9702681	1.0	1.8	1.9	159
TYT 03	707687	9702671	0.6	2.1	4.4	133
TYT_04	707697	9702681	0.8	2.0	3.0	112
TYT_05	707687	9702690	0.8	2.8	5.9	105

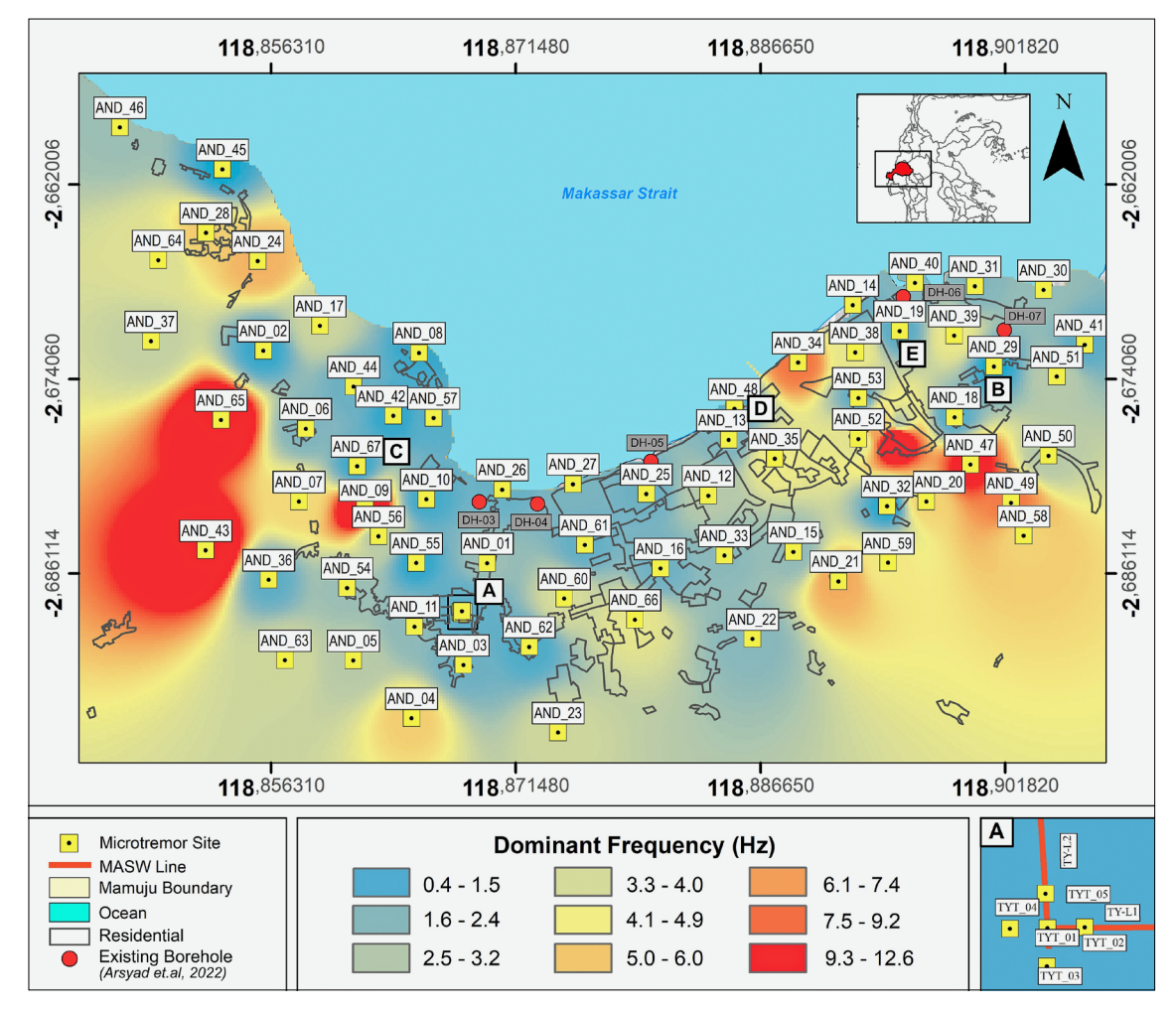


**Figure 4.** Distribution of dominant frequency across the study area from HVSR analysis. **A)** The research site indicated to have experienced liquefaction.

with high dominant frequencies (>10 Hz) are mostly located in the eastern and western parts of the study area, where the terrain has higher elevations compared to sites with low and medium frequencies, this frequency indicates thin sediment layers of less than 5 meters. Relating this to the geological formations in the study area (see Figure 2), sites with low-frequency values are found in the Alluvium Formation, while some are in the Mamuju Formation. According to (Kang et al., 2020; Syamsuddin et al., 2024), the Alluvium Formation consists of lithology that includes sand, gravel, silt, clay, and gravel, which is vulnerable to the destructive impacts of earthquakes, including liquefaction.

#### 3.2. Shear Wave Velocity

Shear wave velocity  $(V_s)$  is an essential parameter for characterizing the dynamic properties of shallow subsurface materials (**Pandavenes et al., 2023**). The average shear wave velocity in the upper 30 meters  $(V_{s30})$  is often used to classify soil types and assess their potential for amplification during an earthquake (**Alkan & Akkaya, 2023**). Lower  $V_{s30}$  values are indicative of softer,

more vulnerable soils, while higher values represent stiffer, less susceptible formations (**Bajaj & Anbazhagan**, 2019; **Kang et al.**, 2021). The distribution of  $V_{s30}$  values can be seen in **Figure 5**.

Based on the HVSR result, the  $V_{s30}$  values obtained are divided into two classifications: soft soil (<175 m/s) and stiff soil (175 – 350 m/s). Areas with  $V_{s30}$  values <175 m/s are predominantly located along the coastline, which are generally more vulnerable to ground wave amplification during an earthquake. In the study area, the Alluvium Formation mostly falls into this category. Alluvium consists of loose and unconsolidated sediments, resulting in lower shear wave velocity values. This indicates that this formation is at a higher risk of experiencing destructive earthquake impacts, such as liquefaction, especially in densely populated areas built on this soil. In contrast, the Mamuju Formation and parts of the Adang Volcanic Formation fall into the medium soil category, with  $V_{s30}$  values ranging from 175 to 350 m/s. These  $V_{s30}$  values are found in areas with higher elevations, although some are also located near the coastline. The lithology of these formations tends to be harder than the Alluvium Formation, which means the defor-

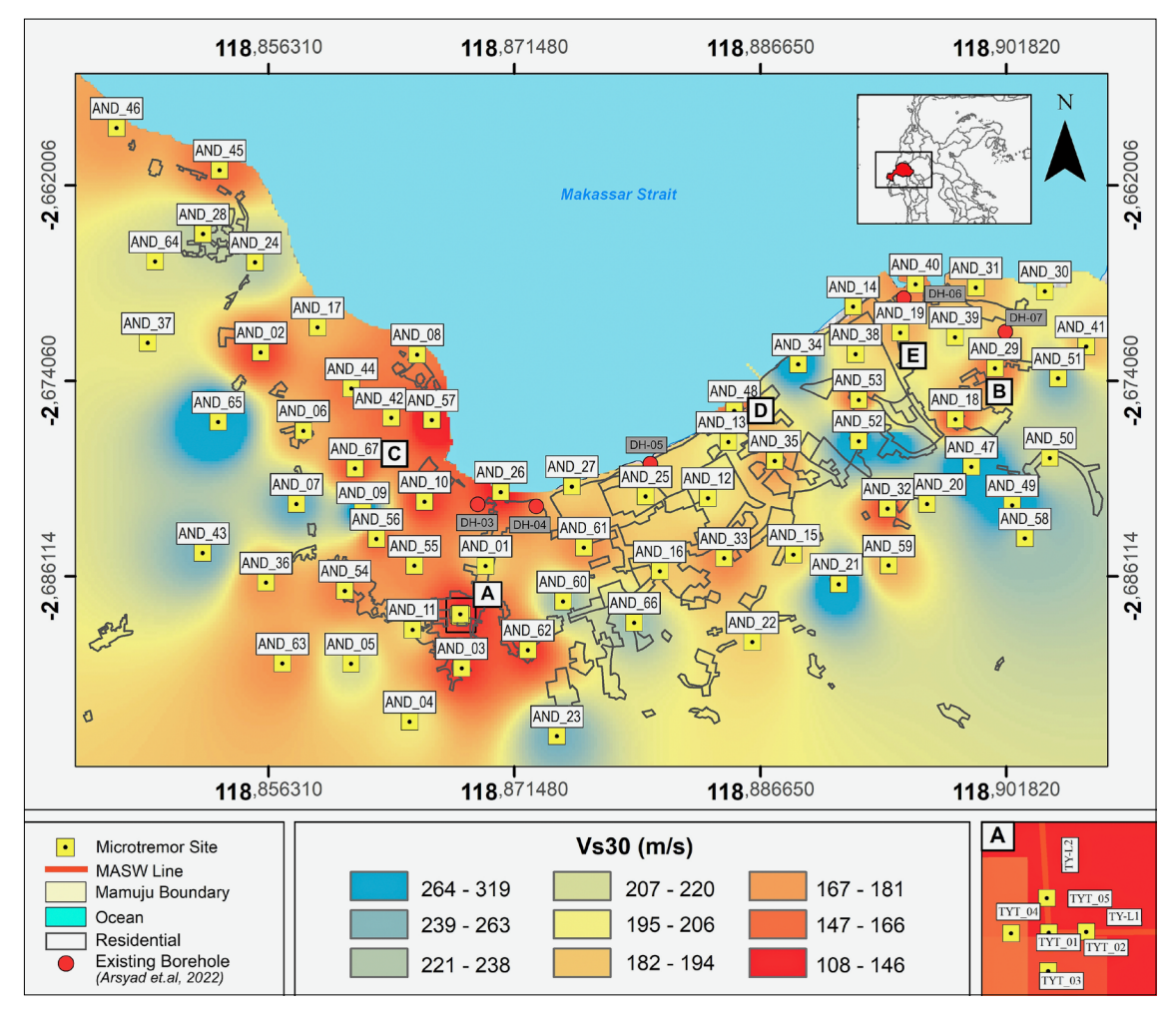


**Figure 5.** Distribution of  $Vs_{30}$  values across the study area from HVSR analysis. **A)** The research site indicated to have experienced liquefaction.

mation caused by earthquakes is likely to be lower. However, despite being less vulnerable to amplification, the presence of discontinuities or weathered zones within these formations can still pose local seismic risks.

In addition to the  $V_{s30}$  values obtained through HVSR inversion, MASW measurements were also conducted at locations identified as having experienced liquefaction during the 2021 earthquake. The  $V_s$  profiles from the MASW measurements are shown in **Figure 6a** and **Figure 6b**. Based on the 2D  $V_s$  profiles from both survey lines, the soil falls into the soft soil category. When compared with the 1D  $V_s$  profiles from HVSR inversion (sites TYT\_01, TYT\_02, TYT\_03, TYT\_04, and TYT\_05), consistency is observed, where the  $V_s$  values at depths of less than 30 meters are low (see **Figure 7**), this indicates that the subsurface sediment layers in this area are relatively thick.

Furthermore, a comparison between  $V_s$  profiles from HVSR and N-SPT values obtained from existing borehole data by **Arsyad et al. (2022)** reveals a consistent trend across several locations, including microtremor sites AND\_26 (near DH-03), AND\_27 (near DH-04), AND 25 (near DH-05), AND 40 (near DH-06), and

AND\_29 (near DH-07). As shown in **Figure 8**, the uppermost layer (0–10 m) exhibits  $V_s < 175$  m/s and N-SPT values below 10, indicating very loose to loose soil characteristics. This layer consists of very loose silty sand (0–8 m) and loose silty sand (8–18 m), which are generally associated with low bearing capacity and high susceptibility to deformation under dynamic loading.

At depths greater than 10 meters,  $V_s$  values exceed 175 m/s, while N-SPT values also increase beyond 10. This trend marks the transition from loose to more compact and consolidated soils. In the 18-44 meters depth range, classified as medium fine sand,  $V_s$  values range between 175 and 350 m/s, accompanied by a gradual increase in N-SPT values. Beyond 44 meters, the subsurface consists of dense to very dense sand, where  $V_s$  values exceed 350 m/s, and N-SPT values continue to rise, reflecting a more stable subsurface condition. The correlation between V and N-SPT is particularly relevant for liquefaction assessment. Previous studies suggest that soils with  $V_s < 200$ m/s and N-SPT < 10 are highly susceptible to liquefaction (Sundararajan & Seshunarayana, 2011). In this study, such conditions are observed in the upper 10 meters, where the soil remains unconsolidated.

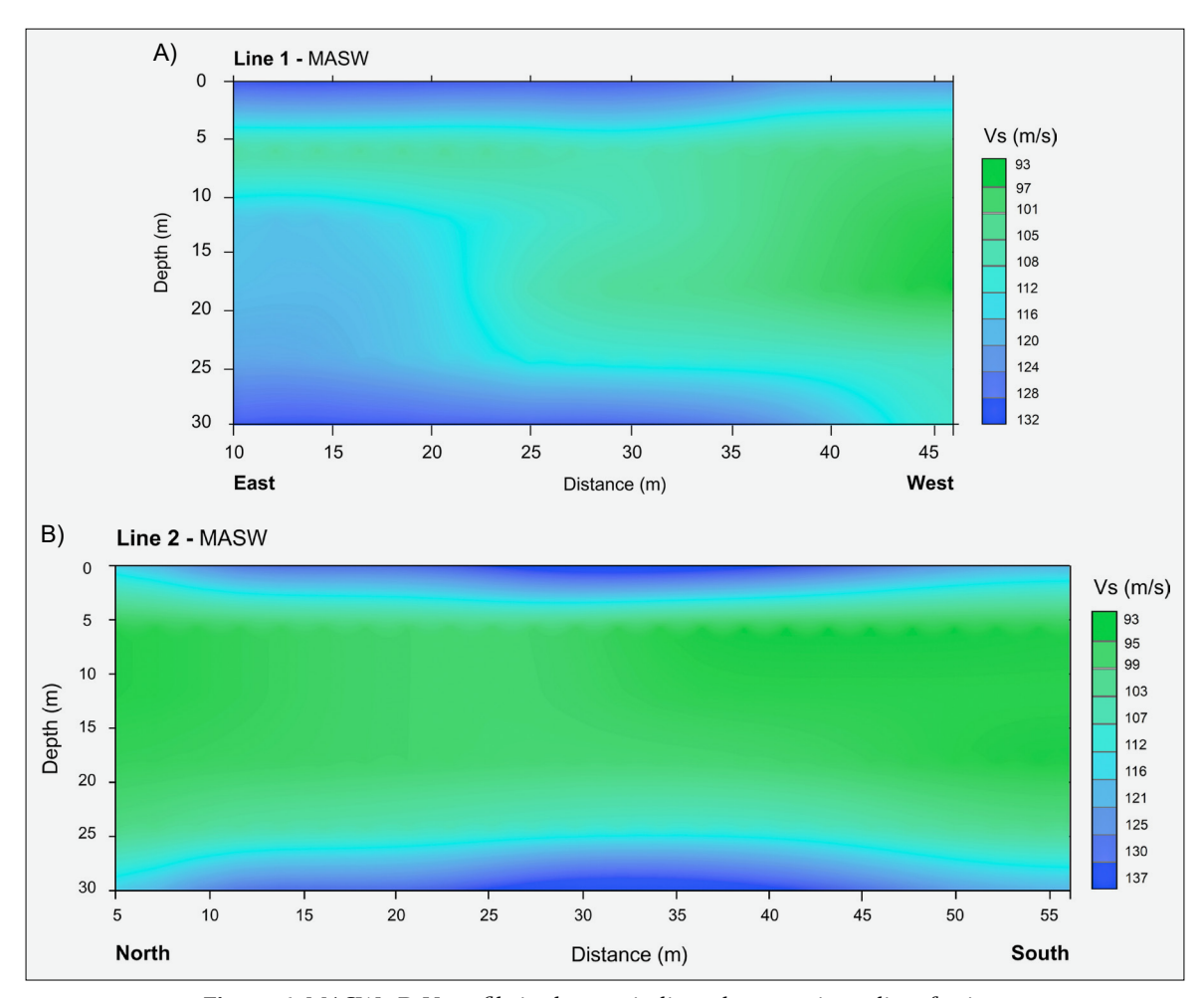


**Figure 6.** MASW 2D  $V_s$  profile in the area indicated to experience liquefaction. **A)** 2D Profile of Line 1 MASW. **B)** 2D Profile of Line 2 MASW.

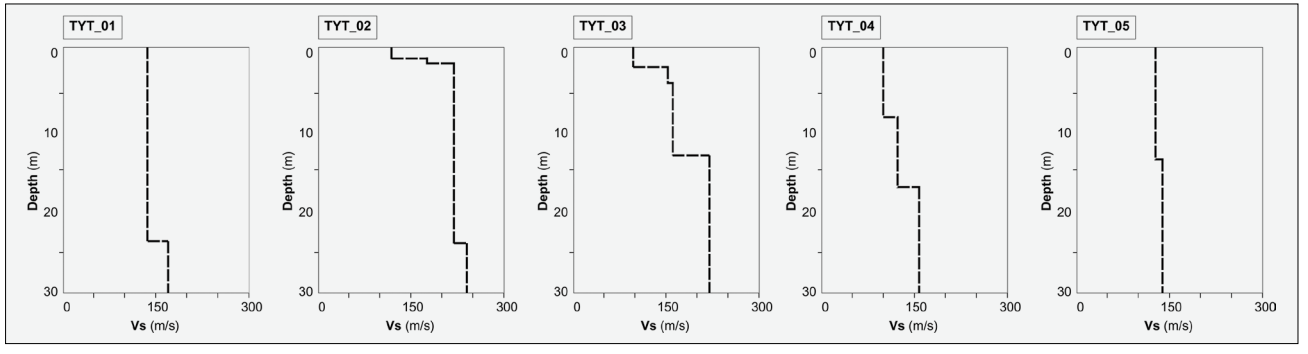


**Figure 7.** 1D  $V_s$  profile from HVSR inversion (station TYT\_01, TYT\_02, TYT\_03, TYT\_04, and TYT\_05) in the liquefaction indicated area.

#### 3.3. Seismic Vulnerability Index

The seismic vulnerability index  $(K_g)$  provides a quantitative measure of a site's susceptibility to seismic shaking, liquefaction, and potential damage (**Pamuk et al., 2018**). It is calculated by relating the amplification factor  $(A_0)$  and the dominant frequency  $(f_0)$ , as seen in **Equation 2**, according to (**Akkaya, 2020; Kang et al., 2021**) higher  $K_g$  values suggest a greater likelihood of ground deformation, liquefaction, and structural damage. The distribution of  $K_g$  values in the study area can be seen in

Figure 9. Areas dominated by the Alluvium Formation, which consists of loose sediments such as sand, clay, and silt, tend to have higher  $K_g$  values, these results are consistent with the findings of (Kang et al., 2021; Syamsuddin et al., 2024). This is due to the Alluvium's susceptibility to deformation and compression, increasing the liquefaction potential, especially in densely populated or infrastructurally significant zones. To further verify these findings, borehole data from previous investigations in Mamuju (Arsyad et al., 2022) were ana-

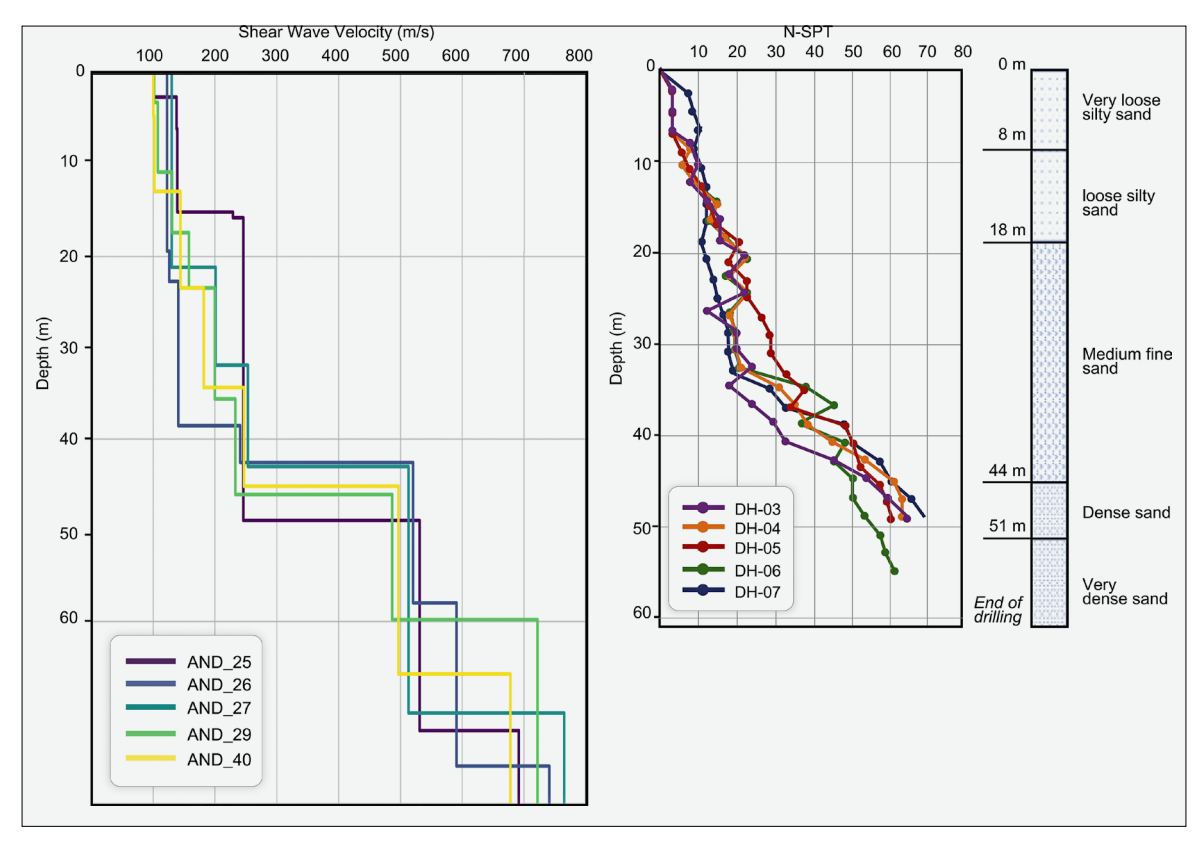


**Figure 8.** Comparison of the  $V_s$  profile derived from HVSR microtremor data (left) and the N-SPT profile from borehole data (right) modified from **Arsyad et al.**, (2022). The  $V_s$  profile represents the shear wave velocity variation with depth, while the N-SPT profile indicates soil resistance based on the standard penetration test. The borehole locations are correlated with nearby HVSR measurement points as follows: DH-03 corresponds to AND\_26, DH-04 to AND\_27, DH-05 to AND\_25, DH-06 to AND\_40, and DH-07 to AND\_29.

lyzed. The geotechnical drillings in coastal areas revealed that the first 8 m consists of very loose silty sands, underlain by 10 m of loose silty sand, followed by 26 m of medium-dense sands and deeper dense to very dense sands. These layers coincide with the areas of high  $K_g$  values, supporting the correlation between sediment characteristics and liquefaction susceptibility. Furthermore, the borehole data indicate that liquefaction thickness could reach up to 16 m during a deterministic Mw 7.0 earthquake with a peak surface acceleration of 0.414g, consistent with the spatial distribution of  $K_g$  values. Additionally, these findings align with the locations of observed liquefaction during the 2021 Mw 6.2 earthquake, where the borehole recorded significant post-liquefaction ground settlement of up to 50 cm.

#### 4. Discussion

The integration of HVSR and MASW methods has proven to be a robust approach for assessing liquefaction susceptibility in Mamuju, West Sulawesi. The results of this study align with existing literature, demonstrating that the combined use of fo,  $V_{s30}$ , and  $K_g$  parameters provides a comprehensive framework for evaluating seismic vulnerability. The low fo values (<2.5 Hz) observed in coastal regions confirm the presence of thick, uncon-

solidated alluvial deposits. These findings are consistent with prior studies (Mirzaoglu & Dýkmen, 2003; Molnar et al., 2022; Pamuk et al., 2018; Quintero et al., 2023; Syamsuddin et al., 2024), which emphasize that low-frequency resonances are indicative of significant sediment thickness and increased susceptibility to liquefaction. The spatial distribution of low fo values aligns closely with areas affected by liquefaction during the 2021 earthquake, further validating the reliability of HVSR analysis in identifying high-risk zones (Syamsuddin et al., 2024). These affected areas correspond to the Alluvium Formation, which is characterized by loose sediments commonly found in lowland areas near the coast and along riverbanks. These water-saturated alluvial layers are highly susceptible to liquefaction due to their ability to deform under seismic loading (Sundararajan & Seshunarayana, 2011).

The  $V_{s30}$  results highlight the critical role of shear wave velocity in characterizing soil stiffness and seismic response (Anbazhagan et al., 2019; Wijayanto et al., 2022). Coastal zones with  $V_{s30}$  values below 175 m/s are dominated by loose alluvial deposits, which amplify seismic waves and significantly increase the risk of ground deformation and liquefaction. This observation corroborates the findings of Bajaj and Anbazhagan (2019), who reported similar amplification effects in soft

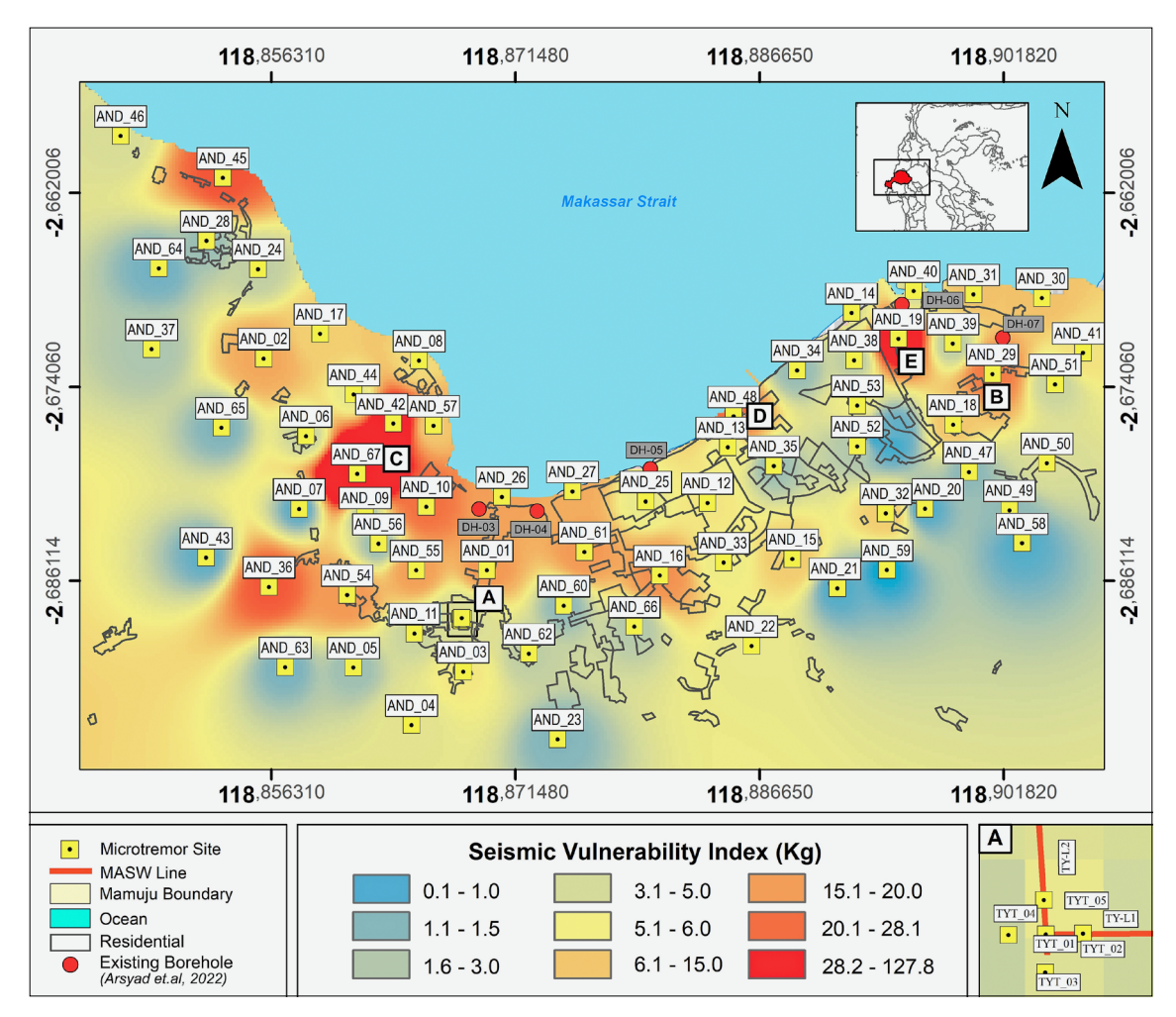


**Figure 9.** Distribution of seismic vulnerability index  $(K_g)$  across the study area from HVSR analysis. A) The research site indicated to have experienced liquefaction.

soils with low  $V_{s30}$  values. In contrast, the higher  $V_{s30}$  values (175-350 m/s) observed in elevated regions, corresponding to the Mamuju and Adang Volcanic formations, suggest greater soil stability. These results demonstrate that  $V_{s30}$  serves as a reliable indicator for distinguishing between areas with varying levels of seismic vulnerability. The MASW measurements in this study were conducted at locations identified as having experienced liquefaction during the 2021 earthquake. This targeted approach ensured that the most vulnerable areas were thoroughly evaluated. The two-dimensional V profiles derived from MASW data revealed soft soil conditions with low shear wave velocities, aligning with the one-dimensional profiles obtained from HVSR inversion. These areas are characterized by thick, unconsolidated sedimentary layers, further confirming their susceptibility to seismic wave amplification and deformation. By focusing on these high-risk zones, the MASW measurements provided critical insight into the spatial variability of subsurface properties, offering a detailed understanding of soil behaviour under seismic loading. This site-specific data not only validated the findings from HVSR but also enhanced the reliability of the microzonation map, reinforcing the importance of integrating multiple geophysical methods for seismic risk assessment.

The  $K_{\alpha}$  parameter further enhances the understanding of liquefaction potential by quantifying the relationship between amplification (A<sub>0</sub>) and dominant frequency (f<sub>0</sub>). The high  $K_{\alpha}$  values (>10) observed in coastal regions correspond to the Alluvium Formation, which consists of unconsolidated sand, silt, clay, and gravel deposits commonly found in lowland areas near the coast and along riverbanks. These loose, water-saturated sediments reinforce their susceptibility to seismic-induced deformation. Previous studies (Alkan & Akkaya, 2023; Kang et al., 2021; Livaoğlu et al., 2019; Putti & Satyam, 2020) have demonstrated that soils with high  $K_a$  values are prone to liquefaction due to their inability to resist dynamic stresses during earthquakes. In contrast, lower  $K_{\alpha}$  values (<10) are predominantly found in the Mamuju Formation and Adang Volcanics, which consist of more compacted geological units with greater shear strength and lower amplification potential. This reinforces the reliability of the  $K_a$  index in identifying liquefaction-prone areas and underscores its role in seismic hazard mitigation. However, while high  $K_{g}$  values often correlate with liquefaction occurrence, exceptions exist where liquefaction is observed in zones with moderate K<sub>a</sub> values, highlighting the influence of additional factors beyond amplification characteristics. Moreover, not all zones with relatively high  $K_a$  values experienced liquefaction after the latest earthquake. For example, at location A, despite being within a zone classified as having moderate  $K_{\sigma}$  values, liquefaction evidence in the form of sand boils on the pavement was observed. This phenomenon can be linked to the  $V_{\rm s}$  profile, which indicates low V<sub>s</sub> values extending beyond 30 meters in depth, suggesting weak soil conditions that, while generally cohesive, may still be susceptible to localized liquefaction under certain stress conditions. Additionally, the presence of a swamp near location A (see Figure 2A) could have influenced subsurface water distribution and pore pressure dynamics, potentially contributing to the occurrence of sand boils in the area. This highlights the importance of considering both geotechnical properties and local environmental factors in assessing liquefaction susceptibility. Given these complexities, integrating  $K_g$  with  $f_0$  and  $V_{s30}$  offers a more comprehensive approach to microzonation and risk assessment, enabling a more detailed evaluation of site response characteristics. By combining these parameters, it becomes possible to refine liquefaction susceptibility mapping and improve the accuracy of seismic hazard assessments, ensuring a more robust framework for future mitigation efforts..

The findings of this study underscore the importance of considering geological and geotechnical factors in urban planning and disaster mitigation strategies. Coastal areas with low  $V_{s30}$ , low  $f_0$ , and high  $K_g$  values are at the greatest risk of liquefaction and require immediate attention for disaster risk reduction, consistent with the findings of **Kang et al. (2021)**. Mitigation measures such as soil stabilization, reinforcement of building foundations, and the implementation of stricter building codes are essential to reduce the potential impact of future seismic events. Additionally, the development of detailed microzonation maps based on these parameters can guide policymakers in identifying high-risk areas and prioritizing resource allocation for disaster preparedness.

While the integration of HVSR and MASW methods has yielded valuable insight, some limitations warrant further investigation. For instance, the accuracy of the  $f_0$  values derived from HVSR is influenced by local variations in sediment properties and environmental noise conditions, as highlighted by **Molnar et al. (2022)**. Similarly, the resolution of  $V_{s30}$  profiles obtained from MASW depends on the spacing and configuration of geophones, which may introduce uncertainties in areas with complex subsurface conditions (**Liu et al., 2020**). Additionally, the presence and depth of groundwater play a crucial role in liquefaction susceptibility, as saturated loose sediments are more prone to excess pore water pressure buildup during seismic events. Areas with a

high water table may exhibit stronger liquefaction effects, whereas drier soils with similar Vs characteristics may not experience the same degree of deformation. Future studies should consider incorporating groundwater measurements alongside geophysical surveys to improve liquefaction assessments. To address these limitations, future research should integrate additional geophysical methods, such as electrical resistivity tomography or borehole logging, to validate and enhance the reliability of the findings.

Moreover, the study highlights the need for further research on the dynamic behaviour of soils under cyclic loading, particularly in regions with complex geological formations like Mamuju. Laboratory testing and numerical modeling can provide deeper insight into the mechanisms of liquefaction and ground deformation, complementing the field-based findings of this study (Abudeif et al., 2019). Such efforts will contribute to the development of more comprehensive seismic hazard assessment frameworks, ultimately improving the resilience of communities in seismically active regions. In summary, the integration of HVSR and MASW methods has provided a detailed characterization of soil properties and seismic vulnerability in Mamuju. The findings not only align with previous research, but also offer practical implications for disaster risk reduction and urban planning. By addressing the limitations and expanding the scope of future studies, this approach can serve as a valuable model for assessing liquefaction potential in other seismically active regions worldwide.

#### 5. Conclusions

This study provides a detailed assessment of liquefaction susceptibility in the Mamuju region, West Sulawesi, using the integrated HVSR and MASW methods to characterize subsurface conditions. The findings confirm that shear wave velocity  $(V_{s30})$ , dominant frequency (fo), and seismic vulnerability index  $(K_g)$  are strongly correlated with underlying geological formations, significantly influencing the region's seismic response. The findings confirm that variations in shear wave velocity  $(V_{s,0})$ , dominant frequency (fo), and seismic vulnerability index  $(K_{\alpha})$  correspond closely with underlying geological formations, influencing the region's seismic response. Areas underlain by unconsolidated alluvial deposits, which exhibit low  $V_{s30}$ , low fo, and high  $K_g$  values, are identified as highly susceptible to liquefaction due to their low shear strength and significant ground motion amplification. In contrast, the Mamuju and Adang Volcanic formations, with higher  $V_{s30}$  and fo values and lower  $K_g$ , indicate more stable subsurface conditions with reduced seismic amplification. The spatial distribution of these parameters aligns with ground failures observed during the 2021 Mamuju earthquake (Mw 6.2), reinforcing the reliability of geophysical methods in identifying highrisk zones. The results underscore the importance of integrating seismic microzonation approaches in earthquake-prone regions, providing critical insight for refining seismic hazard models and improving disaster mitigation strategies.

### Acknowledgement

The authors would like to thank all those who have contributed to this research. This research was supported by the Ministry of Education, Culture, Research, and Technology Indonesia (BIMA Research Program 2024) and LP2M Hasanuddin University. The authors would also like to thank BMKG and the Geophysics Department Surveyor Team (Muhammad Syaifullah, Hasnan Sutadi, Wirawan Saleh, and Ahmad Fauzy Arif) for microtremor and MASW data acquisition in the field.

#### **Funding**

This research was funded by the Ministry of Education, Culture, Research, and Technology Indonesia, BIMA Research Program 2024, grant number [0459/E5/PG.02.00/2024].

### 6. References

- Abudeif, A. M., Fat-Helbary, R. E., Mohammed, M. A., Alkhashab, H. M., & Masoud, M. M. (2019). Geotechnical engineering evaluation of soil utilizing 2D multichannel analysis of surface waves (MASW) technique in New Akhmim city, Sohag, Upper Egypt. *Journal of African Earth Sciences*, 157, 103512. https://doi.org/10.1016/j.jafrearsci.2019.05.020
- Ahn, J., Kwak, Y. D., & Kim, H. (2021). Estimating VS30 at Korean Peninsular seismic observatory stations using HVSR of event records. *Soil Dynamics and Earthquake Engineering*, *146*(106650), 1–20. https://doi.org/10.1016/j. soildyn.2021.106650
- Akkaya, İ. (2020). Availability of Seismic Vulnerability Index (Kg) in The Assessment if Building Damage in Van, Eastern Turkey. Earthquake Engineering and Engineering Vibration, 19(1), 189–204.
- Alan, Y., Antony, M., & John, B. (2019). Precision of V S 30 values derived from noninvasive surface wave methods at 31 sites in California. *Soil Dynamics and Earthquake Engineering*, 127, 105802. https://doi.org/10.1016/j.soil-dyn.2019.105802
- Alkan, A., & Akkaya, İ. (2023). Investigation of site properties of the Çaldıran (Van, Eastern Turkey) settlement area using surface wave and microtremor methods. *Journal of African Earth Sciences*, 197, 104737. https://doi.org/10. 1016/j.jafrearsci.2022.104737
- Anbazhagan, P., Srilakshmi, K. N., Bajaj, K., Moustafa, S. S. R., & Al-Arifi, N. S. N. (2019). Determination of seismic site classification of seismic recording stations in the Himalayan region using HVSR method. *Soil Dynamics and Earthquake Engineering*, 116, 304–316. https://doi.org/10.1016/j.soildyn.2018.10.023

- Ardianto, A., Anggayana, K., Widayat, A. H., Sasongko, D., & Fakhruddin, R. (2024). Energy Geoscience Organic geochemical, petrographic and palynological characterization of claystones of the Palaeogene Toraja Formation, and oil seeps in the Enrekang Sub-basin, south Sulawesi, Indonesia: Implications for hydrocarbon source rock poten. Energy Geoscience, 5. https://doi.org/10.1016/j.engeos. 2024.100287
- Arsyad, A., Asti, A., Amaliyah, N., Paerong, S., & Djamaluddin, A. R. (2022). Liquefaction Potential Assessment for the City of Mamuju Sulawesi by using N-SPT based methods. *Indonesian Geotechnical Journal*, *1*(3), 37–55.
- Bajaj, K., & Anbazhagan, P. (2019). Seismic site classi fi cation and correlation between V S and SPT-N for deep soil sites in Indo-Gangetic Basin. *Journal of Applied Geophysics*, *163*, 55–72. https://doi.org/10.1016/j.jappgeo.2019.02.011
- Bao, X., Jin, Z., Cui, H., Chen, X., & Xie, X. (2019). Soil Liquefaction Mitigation in Geotechnical Engineering: An Overview of Recently Developed Methods. *Soil Dynamics* and Earthquake Engineering, 120(January), 273–291. https://doi.org/10.1016/j.soildyn.2019.01.020
- Bignardi, S. (2017). The uncertainty of estimating the thickness of soft sediments with the HVSR method: A computational point of view on weak lateral variations. *Journal of Applied Geophysics*, 145, 28–38. https://doi.org/10.1016/j.jappgeo.2017.07.017
- BMKG. (2021). Preliminary report on the M6.2 earthquake survey in Mamuju-Majene, January 16–22, 2021.
- Chaloulos, Y. K., Giannakou, A., Drosos, V., Tasiopoulou, P., Chacko, J., & de Wit, S. (2020). Liquefaction-induced settlements of residential buildings subjected to induced earthquakes. Soil Dynamics and Earthquake Engineering, 129, 105880. https://doi.org/10.1016/j.soildyn.2019.105880
- Chávez-García, F. J., & Raptakis, D. (2017). Local amplification and subsoil structure at a difficult site: Understanding site effects from different measurements. *Soil Dynamics and Earthquake Engineering*, *92*, 334–344. https://doi.org/10.1016/j.soildyn.2016.10.008
- Chiaradonna, A., Spadi, M., Monaco, P., Papasodaro, F., & Tallini, M. (2022). Seismic Soil Characterization to Estimate Site Effects Induced by Near-Fault Earthquakes: The Case Study of Pizzoli (Central Italy) during the Mw 6.7 2 February 1703, Earthquake. *Geosciences*, *12*(2), 1–33. https://doi.org/. https://doi.org/10.3390/geosciences12010002
- Fat-Helbary, R. E. S., El-Faragawy, K. O., & Hamed, A. (2019). Application of HVSR technique in the site effects estimation at the south of Marsa Alam city, Egypt. *Journal of African Earth Sciences*, *154*, 89–100. https://doi.org/10.1016/j.jafrearsci.2019.03.015
- Foti, S., Lai, C. G., Rix, G. J., & Strobbia, C. (2015). Surface Wave Methods for Near-Surface Site Characterization. In CRC Press. Surface-Wave-Methods-Near-Surface-Characterization/dp/0415678765
- Ghione, F., Köhler, A., Dichiarante, A. M., Aarnes, I., & Oye, V. (2023). Vs30 and depth to bedrock estimates from integrating HVSR measurements and geology-slope approach in the Oslo area, Norway. *Frontiers in Earth Science*, *11*(1242679), 1–19. https://doi.org/10.3389/feart. 2023.1242679

- Griffiths, S. C., Cox, B. R., Rathje, E. M., & Teague, D. P. (2016). Mapping Dispersion Misfit and Uncertainty in Vs Profiles to Variability in Site Response Estimates. *Journal of Geotechnical and Geoenvironmental Engineering*, 142(11), 1–12. https://doi.org/10.1061/(ASCE)GT.1943-5606.0001553.
- Gupta, R. K., Agrawal, M., Pal, S. K., & Das, M. K. (2021). Seismic site characterization and site response study of Nirsa (India). *Natural Hazards*, 0123456789. https://doi. org/10.1007/s11069-021-04767-w
- Hanifa, N. R., Gunawan, E., Firmansyah, S., Faizal, L., Retnowati, D. A., Pradipta, G. C., Imran, I., & Lassa, J. A. (2022). Unmanned Aerial Vehicles for geospatial mapping of damage assessment: A study case of the 2021 Mw 6.2 Mamuju-Majene, Indonesia, earthquake during the coronavirus disease 2019 (COVID-19) pandemic. Remote Sensing Applications: Society and Environment, 28(August), 100830. https://doi.org/10.1016/j.rsase.2022.100830
- Hanindya, K. A., Makrup, L., Widodo, & Paulus, R. (2023). Deterministic Seismic Hazard Analysis to Determine Liquefaction Potential Due to Earthquake. *Civil Engineering Journal*, 9(05), 1203–1216.
- Hossain, M. S., Kamal, A. S. M. M., Rahman, M. Z., Farazi, A. H., Mondal, D. R., Mahmud, T., & Ferdous, N. (2020).
  Assessment of soil liquefaction potential: a case study for Moulvibazar town, Sylhet, Bangladesh. SN Applied Sciences, 2(777), 1–12. https://doi.org/10.1007/s42452-020-2582-x
- Ismail, A., Denny, F. B., & Metwaly, M. (2014). Comparing Continuous Profiles from MASW and Shear-wave Reflection Seismic Methods. *Journal of Applied Geophysics*, 105, 67–77. https://doi.org/10.1016/j.jappgeo.2014.03.007
- Kang, S. Y., Kim, K. H., Chiu, J. M., & Liu, L. (2020). MicrotremorHVSR analysis of heterogeneous shallow sedimentary structures at Pohang, South Korea. *Journal of Geophysics and Engineering*, 17(5), 861–869. https://doi.org/10.1093/jge/gxaa035
- Kang, S. Y., Kim, K. H., & Kim, B. (2021). Assessment of seismic vulnerability using the horizontal-to-vertical spectral ratio (HVSR) method in Haenam, Korea. *Geosciences Journal*, 25(1), 71–81. https://doi.org/10.1007/s12303-020-0040-9
- Khalili, M., & Mirzakurdeh, A. V. (2019). Fault detection using microtremor data (HVSR-based approach) and electrical resistivity survey. *Journal of Rock Mechanics and Geotechnical Engineering*, 11(2), 400–408. https://doi.org/10.1016/j.jrmge.2018.12.003
- Kusmanto, Ismanti, S., & Setiawan, A. F. (2024). Assessment of liquefaction risk with unidentified seismic parameters for newly-discovered faults: numerical analysis. *International Journal of GEOMATE*, 26(114), 50–59.
- Liu, H., Maghoul, P., Shalaby, A., Bahari, A., & Moradi, F. (2020). Integrated approach for the MASW dispersion analysis using the spectral element technique and trust region reflective method. *Computers and Geotechnics*, 125, 103689. https://doi.org/10.1016/j.compgeo.2020.103689
- Livaoğlu, H., Irmak, T. S., & Güven, I. T. (2019). Seismic vulnerability indices of ground for Değirmendere (Kocaeli Province, Turkey). *Bulletin of Engineering Geology and*

- the Environment, 78(1), 507–517. https://doi.org/10.1007/s10064-017-1102-8
- Ma, N., Wang, G., Kamai, T., Doi, I., & Chigira, M. (2019). Amplification of seismic response of a large deep-seated landslide in Tokushima, Japan. *Engineering Geology*, 249, 218–234. https://doi.org/10.1016/j.enggeo.2019.01.002
- Maghami, S., Sohrabi-bidar, A., Bignardi, S., Zarean, A., & Kamalian, M. (2021). Extracting the shear wave velocity structure of deep alluviums of "Qom" Basin (Iran) employing HVSR inversion of microtremor recordings. *Journal of Applied Geophysics*, *185*(104246), 1–19. https://doi.org/10.1016/j.jappgeo.2020.104246
- Mahajan, A. K., Mundepi, A. K., Chauhan, N., Jasrotia, A. S., Rai, N., & Kumar, T. (2012). Active seismic and passive microtremor HVSR for assessing site effects in Jammu city, NW Himalaya, India - A case study. *Journal of Applied Geophysics*, 77, 51–62. https://doi.org/10.1016/j.jappgeo.2011.11.005
- Mahmoud, A. O., Hussien, M. N., Karray, M., Chekired, M., Bessette, C., & Jinga, L. (2020). Mitigation of liquefaction-induced uplift of underground structures. *Computers* and Geotechnics, 125, 103663. https://doi.org/10.1016/j. compgeo.2020.103663
- Maklad, M., Yokoi, T., Hayashida, T., ElGabry, M. N., Hassan, H. M., Hussein, H. M., Fattah, T. A., & Rashed, M. (2020). Site characterization in Ismailia, Egypt using seismic ambient vibration array. *Engineering Geology*, 279, 105874. https://doi.org/10.1016/j.enggeo.2020.105874
- Mase, L. Z., Likitlersuang, S., Tobita, T., Chaiprakaikeow, S., & Soralump, S. (2018). Local Site Investigation of Liquefied Soils Caused by Earthquake in Northern Thailand. *Journal of Earthquake Engineering*, 00(00), 1–24. https://doi.org/10.1080/13632469.2018.1469441
- Meilano, I., Salman, R., Susilo, S., Shiddiqi, H. A., Supendi, P., Lythgoe, K., Tay, C., Bradley, K., Rahmadani, S., Kristyawan, S., & Yun, S. H. (2023). The 2021 MW6.2 Mamuju, West Sulawesi, Indonesia earthquake: partial rupture of the Makassar Strait thrust. *Geophysical Journal International*, 233(3), 1694–1707. https://doi.org/10.1093/gji/ggac512
- Mihaylov, A., El Naggar, H., Mihaylov, D., & Dineva, S. (2019). Approximate analytical HVSR curve using multiple band-pass filters and potential applications. *Soil Dynamics and Earthquake Engineering*, 127. https://doi.org/10.1016/j.soildyn.2019.105840
- Mirzaoglu, M., & Dýkmen, Ü. (2003). Application of Microtremors to Seismic Microzoning Procedure. *Journal of the balkan geophysical society*, *6*(3), 143–156.
- Mohammed, M. A., Abudeif, A. M., & Abd el-aal, A. K. (2020). Engineering geotechnical evaluation of soil for foundation purposes using shallow seismic refraction and MASW in 15th Mayo, Egypt. *Journal of African Earth Sciences*, 162, 103721. https://doi.org/10.1016/j.jafrears-ci.2019.103721
- Molnar, S., Sirohey, A., Assaf, J., Bard, P. Y., Castellaro, S., Cornou, C., Cox, B., Guillier, B., Hassani, B., Kawase, H., Matsushima, S., Sánchez-Sesma, F. J., & Yong, A. (2022). A review of the microtremor horizontal-to-vertical spectral

- ratio (MHVSR) method. *Journal of Seismology*, 26, 653–685. https://doi.org/10.1007/s10950-021-10062-9
- Moon, S. W., Subramaniam, P., Zhang, Y., Vinoth, G., & Ku, T. (2019). Bedrock depth evaluation using microtremor measurement: empirical guidelines at weathered granite formation in Singapore. *Journal of Applied Geophysics*, 171, 103866. https://doi.org/10.1016/j.jappgeo.2019.103866
- Najaftomarei, M. R., Rahimi, H., Tanircan, G., Mahani, A. B., & Shahvar, M. (2020). Site classification and probabilistic estimation of Vs30 for the Iranian strong-motion network. *Physics of the Earth and Planetary Interiors*, *308*, 106583. https://doi.org/10.1016/j.pepi.2020.106583
- Nakamura, Y. (2000). Clear Identification of Fundamental Idea of Nakamura's Technique and Its Applications. *The 12th World Conference on Earthquake Engineering*, 2656, 1–8.
- Nguyen-Tien, H., Nguyen-Hong, P., Nguyen-Le, M., Che-Min, L., Tran-An, N., Pham-The, T., & Nguyen-Van, D. (2022). Establishment of the correlation between the near-surface sedimentary thickness and the microtremor dominant frequency in the Hanoi area. 45(1), 49–66. https://doi.org/https://doi.org/10.15625/2615-9783/17569
- Odom, W., & Doctor, D. (2023). Applied Computing and Geosciences Rapid estimation of minimum depth-to-bedrock from lidar leveraging deep-learning-derived surficial material maps. *Applied Computing and Geosciences*, 18, 1–11. https://doi.org/10.1016/j.acags.2023.100116
- Pamuk, E., Özdağ, Ö. C., Tunçel, A., Özyalın, Ş., & Akgün, M. (2018). Local site effects evaluation for Aliağa/İzmir using HVSR (Nakamura technique) and MASW methods. Natural Hazards, 90(2), 887–899. https://doi.org/10.1007/s11069-017-3077-y
- Pandavenes, O. A., Bernal, D., & Torrijo, F. J. (2023). A Comparative Analysis for Defining the Sliding Surface and Internal Structure in an Active Landslide Using the HVSR Passive Geophysical Technique in Pujilí (Cotopaxi), Ecuador. *Land*, 12(961), 1–29. https://doi.org/https://doi.org/10.3390/land12050961
- Perdana, M. J., & Amijaya, H. (2011). Source indication of oil seep from paniki river, kalukku, mamuju, west sulawesi based on geochemical characterization. *Proceedings JCM Makassar* 2011.
- Perez, C. J. A. (2024). Reevaluating soil amplification using multi spectral HVSR technique in La Chana Neighborhood, Granada, Spain. *Journal of Seismology*, 28(4), 921–949. https://doi.org/10.1007/s10950-024-10227-2
- Piña-flores, J., Cárdenas-soto, M., García-jerez, A., Seivane, H., Luzón, F., & Sánchez-sesma, F. J. (2020). Use of peaks and troughs in the horizontal-to-vertical spectral ratio of ambient noise for Rayleigh-wave dispersion curve picking. *Journal of Applied Geophysics*, 177, 104024. https:// doi.org/10.1016/j.jappgeo.2020.104024
- Putti, S. P., & Satyam, N. (2020). Evaluation of Site Effects Using HVSR Microtremor Measurements in Vishakhapatnam (India). Earth Systems and Environment, 4(2), 439– 454. https://doi.org/10.1007/s41748-020-00158-6
- Qadri, S. M. T., Sajjad, S. H., Sheikh, R. A., Rehman, K., Rafi, Z., Nawz, B., & Haider, W. (2015). Ambient noise meas-

- urements in Rawalpindi Islamabad , twin cities of Pakistan: a step towards site response analysis to mitigate impact of natural hazard. *Natural Hazards*, 78, 1111-1123. https://doi.org/10.1007/s11069-015-1760-4
- Quintero, J., Gomes, R. C., Rios, S., Ferreira, C., & Viana da Fonseca, A. (2023). Liquefaction assessment based on numerical simulations and simplified methods: A deep soil deposit case study in the Greater Lisbon. *Soil Dynamics* and Earthquake Engineering, 169, 107866. https://doi. org/10.1016/j.soildyn.2023.107866
- Ritonga, R., Maulana, A., & Tonggiroh, A. (2021). Rare Earth Elements Distribution in Weathered Volcanic Rock from Mamuju Area, West Sulawesi. *IOP Conference Series: Earth and Environmental Science*, 921(1). https://doi.org/10.1088/1755-1315/921/1/012039
- Rosianna, I., Nugraha, E. D., Syaeful, H., Putra, S., Hosoda, M., Akata, N., & Tokonami, S. (2020). Natural radioactivity of laterite and volcanic rock sample for radioactive mineral exploration in mamuju, indonesia. *Geosciences (Switzerland)*, 10(9), 1–13. https://doi.org/10.3390/geosciences10090376
- Rosianna, I., Nugraha, E. D., Tazoe, H., Syaeful, H., Muhammad, A. G., Sukadana, I. G., Indrastomo, F. D., Ngadenin, Pratiwi, F., Sumaryanto, A., Sucipta, Pratama, H. A., Mustika, D., Nirwani, L., Nurokhim, Omori, Y., Hosoda, M., Akata, N., & Tokonami, S. (2023). Uranium Isotope Characterization in Volcanic Deposits in a High Natural Background Radiation Area, Mamuju, Indonesia. *Geosciences (Switzerland)*, 13(12), 1–13. https://doi.org/10.3390/geosciences13120388
- Rosid, M. S., Ali, Y. H., & Ramdhan, M. (2022). Characterization of the Mamasa Earthquake Source Based on Hypocenter Relocation and Gravity Derivative Data Analysis. *International Journal of GEOMATE*, 23(97), 220–227. https://doi.org/10.21660/2022.97.j2375
- Roy, J., Rollins, K. M., Athanasopoulos-Zekkos, A., Harper, M., Linton, N., Basham, M., Greenwood, W., & Zekkos, D. (2022). Gravel liquefaction assessment using dynamic cone penetration and shear wave velocity tests based on field performance from the 1964 Alaska earthquake. Soil Dynamics and Earthquake Engineering, 160, 107357. htt-ps://doi.org/10.1016/j.soildyn.2022.107357
- Salleh, A. N., Muztaza, N. M., Sa'ad, R., Zakaria, M. T., Mahmud, N., Rosli, F. N., & Samsudin, N. (2021). Application of geophysical methods to evaluate soil dynamic properties in Penang Island, Malaysia. *Journal of Asian Earth Sciences*, 207(July 2020), 104659. https://doi.org/10.1016/j.jseaes.2020.104659
- Sana, H., & Nath, S. K. (2016). Liquefaction potential analysis of the Kashmir valley alluvium, NW Himalaya. Soil Dynamics and Earthquake Engineering, 85, 11–18. https:// doi.org/10.1016/j.soildyn.2016.03.009
- Sedaghati, F., Pezeshk, S., & Nazemi, N. (2018). Site amplification within the Mississippi embayment of the central United States: Investigation of possible differences among various phases of seismic waves and presence of basin waves. Soil Dynamics and Earthquake Engineering, 113, 534–544. https://doi.org/10.1016/j.soildyn.2018.04.017

- Senkaya, G. V., Senkaya, M., Karsli, H., & Güney, R. (2019). Integrated Shallow Seismic Imaging of a Settlement Located in a Historical Landslide Area. *Bulletin of Engineering Geology and the Environment*.
- Sesame, E. P. (2004). Guidelines for The Implementation Of The H/V Spectral Ratio Technique on Ambient Vibrations Measurements, Processing and Interpretation. European Commission Research General Directorate.
- Shaban, G., Fadlin, & Priadi, B. (2016). Geochemical signatures of potassic to sodic Adang Volcanics, Western Sulawesi: Implications for their tectonic setting and origin. *Indonesian Journal on Geoscience*, 3(3), 195–216. https://doi.org/10.17014/ijog.3.3.195-214
- Shelley, E. O., Mussio, V., Rodríguez, M., & Chang, J. G. A. (2015). Evaluation of soil liquefaction from surface analysis. *Geofísica Internacional*, *54*(1), 95–109. https://doi.org/10.1016/j.gi.2015.04.005
- Simons, W. J. F., Socquet, A., Vigny, C., Ambrosius, B. A. C., Abu, S. H., Promthong, C., Subarya, C., Sarsito, D. A., Matheussen, S., Morgan, P., & Spakman, W. (2007). A decade of GPS in Southeast Asia: Resolving Sundaland motion and boundaries. *Journal of Geophysical Research:* Solid Earth, 112(6). https://doi.org/10.1029/2005JB003868
- Sivaram, K., Gupta, S., Kumar, S., & Prasad, B. N. V. (2018). Shear velocity structural characterization around the Lonar crater using joint inversion of ambient noise HVSR and Rayleigh wave dispersion. *Journal of Applied Geophysics*, 159, 773–784. https://doi.org/10.1016/j.jappgeo.2018.10.022
- Sompotan, A. F. (2012). *Struktur Geologi Sulawesi*. Bandung Institute of Technology.
- Sukkarak, R., Tanapalungkorn, W., Likitlersuang, S., & Ueda, K. (2021). Liquefaction analysis of sandy soil during strong earthquake in Northern Thailand. *Soils and Foundations*, 61(5), 1302–1318. https://doi.org/10.1016/j.sandf.2021.07.003
- Sundararajan, N., & Seshunarayana, T. (2011). Liquefaction Hazard Assessment of Earth Quake Prone Area: a Study Based on Shear Wave Velocity by Multichannel Analysis of Surface Waves (MASW). *Geotechnical and Geological Engineering*, 29, 267–275. https://doi.org/10.1007/s10706-010-9360-2
- Supendi, P., Ramdhan, M., Priyobudi, Sianipar, D., Wibowo, A., Gunawan, M. T., Rohadi, S., Riama, N. F., Daryono, Prayitno, B. S., Murjaya, J., Karnawati, D., Meilano, I., Rawlinson, N., Widiyantoro, S., Nugraha, A. D., Marliyani, G. I., Palgunadi, K. H., & Elsera, E. M. (2021). Foreshock—mainshock—aftershock sequence analysis of the 14 January 2021 (Mw 6.2) Mamuju—Majene (West Sulawesi, Indonesia) earthquake. *Earth, Planets and Space*, 73(1), 1–10. https://doi.org/10.1186/s40623-021-01436-x
- Syamsuddin, E., Maulana, A., Hamzah, A., & Irvan, U. R. (2024). Assessing soil vulnerability in Petobo post-lique-

- faction zone, Palu, Central Sulawesi: A microzonation study utilizing microtremor measurements. *Journal of Degraded and Mining Lands Management*, 11(3), 5805–5816. https://doi.org/10.15243/jdmlm.2024.113.5805
- Tabrizi-Zarringhabaei, S., Ejlali, R. G., Fard, M. Y., & Sayyed-fattahi, S. (2019). A new approach for particle size characterization of soil based on dynamic image analysis (Dia). *Rudarsko-Geološko-Naftni Zbornik*, 34(4), 89–96. https://doi.org/10.17794/rgn.2019.4.9
- TERRADAT. (2024). MASW (Surface Wave Surveys). Terra-Dat.
- Uyanık, O. (2020). Soil liquefaction analysis based on soil and earthquake parameters. *Journal of Applied Geophysics*, *176*, 104004. https://doi.org/10.1016/j.jappgeo.2020.104004
- Wathelet, M., Jongmans, D., & Ohrnberger, M. (2004). Surface-wave inversion using a direct search algorithm and its application to ambient vibration measurements. *Near Surface Geophysics*, 2(4), 211–221. https://doi.org/10.3997/1873-0604.2004018
- White, L. T., Hall, R., Armstrong, R. A., Barber, A. J., Boudagher, M., Baxter, A., Wakita, K., Manning, C., & Soesilo, J. (2017). Journal of Asian Earth Sciences The geological history of the Latimojong region of western Sulawesi, Indonesia. *Journal of Asian Earth Sciences*, 138, 72–91. https://doi.org/10.1016/j.jseaes.2017.02.005
- Wijayanto, Mardiatno, D., Nehren, U., Marfai, M. A., & Pramono, S. (2022). Spatial Distribution of Vs30 Based on MASW and Microtremor Inversion in Gunungkidul, Yogyakarta, Indonesia. *International Journal of GEO-MATE*, 22(94), 29–38. https://doi.org/https://doi.org/10. 21660/2022.94.2463
- Yaghmaei-Sabegh, S., & Rupakhety, R. (2020). A new method of seismic site classification using HVSR curves: A case study of the 12 November 2017 Mw 7.3 Ezgeleh earthquake in Iran. *Engineering Geology*, 270, 105574. https://doi.org/10.1016/j.enggeo.2020.105574
- Yang, S., Mavroeidis, G. P., de la Llera, J. C., Poulos, A., Aguirre, P., Rahpeyma, S., Sonnemann, T., & Halldorsson, B. (2019). Empirical site classification of seismological stations in Chile using horizontal-to-vertical spectral ratios determined from recordings of large subduction-zone earth-quakes. Soil Dynamics and Earthquake Engineering, 125, 105678. https://doi.org/10.1016/j.soildyn.2019.05.017
- Zaidani, M. A., Priadi, B., Sucipta, I. G. B. E., Susanto, V., & Saepuloh, A. (2023). Petrogenesis of Adang and Talaya volcanic rocks, in the Mamuju area and its surrounding, West Sulawesi. *IOP Conference Series: Earth and Environmental Science*, 1245(1). https://doi.org/10.1088/1755-1315/1245/1/012029
- Zhou, Y. G., Xia, P., Ling, D. S., & Chen, Y. M. (2020). Lique-faction case studies of gravelly soils during the 2008 Wenchuan earthquake. *Engineering Geology*, 274, 105691. https://doi.org/10.1016/j.enggeo.2020.105691

#### **SAŽETAK**

# Procjena podložnosti na pojavu likvefakcije pomoću HVSR i MASW metode: studija slučaja Mamuju, Zapadni Sulawesi, Indonezija

Potres koji je pogodio Mamuju 2021. godine (Mw 6,2) istaknuo je veliku ranjivost regije na likvefakciju zbog blizine aktivnih tektonskih zona, prisutnosti holocenskih aluvijalnih naslaga, nekonsolidiranih sedimentnih formacija i tla zasićenoga vodom, što sve pridonosi podložnosti zbog seizmičke aktivnosti. Ovo istraživanje procjenjuje podložnosti na likvefakciju područja Mamuju korištenjem integriranoga pristupa koji kombinira metodu omjera horizontalnoga i vertikalnoga spketra (HVSR) i metodu višekanalne analize površinskih valova (MASW). Ova studija istražuje inverznu korelaciju između  $V_{s30}$  i indeksa seizmičke ranjivosti ( $K_g$ ), gdje niže vrijednosti  $V_{s30}$  odgovaraju višim vrijednostima  $K_g$ , što upućuje na povećanu podložnost na pojavu likvefakcije. HVSR analiza pokazala je kako se dominantna frekvencija ( $f_0$ ) kreće od 0,4 do 11 Hz, dok faktor amplifikacije ( $A_0$ ) varira između 1,1 i 11. Rezultati upućuju na to da obalna područja s debljim aluvijalnim naslagama pokazuju najniže vrijednosti  $f_0$  (<2,5 Hz), koje koreliraju s  $V_{s30}$  < 175 m/s i  $K_g$  > 10, a što upućuje na veću vjerojatnost pojave likvefakcije. Nasuprot tome, područja ispod formacije Mamuju i vulkana Adang okarakterizirana su višim vrijednostima  $V_{s30}$  (>175 m/s),  $f_0$  (>10 Hz) i  $K_g$  (<10) te upućuju na manju vjerojatnost pojave likvefakcije. Ova saznanja pridonose razvoju detaljne karte mikrozoniranja nužne za definiranje rizika od likvefakcije, što je važno ako se želi unaprijediti urbanističko planiranje i ublažavanje katastrofa u Mamujuu. Predmetno istraživanje pokazalo je kako integracija HVSR i MASW metoda predstavlja pouzdan pristup pri karakterizaciji svojstava tla, kao i unaprijeđenje procjene rizika od pojave likvefakcije u seizmički aktivnim regijama.

#### Ključne riječi:

likvefakcija, HVSR metoda, MASW metoda, indeks seizmičke ranjivosti, brzina posmičnih valova, potres u Mamujuu

## Author's contribution

**Andri Moh. Wahyu Laode** (S.Si, Geophysics Master Degree Student) contributed to data collection, processing, interpretation, and drafting the original manuscript. **Muh. Altin Massinai** (Prof., Professor of Geophysics Department) supervised the research, provided critical discussions on methodology, and reviewed the manuscript. **Muh. Fawzy Imsullah Massinai** (M.T.) contributed to data interpretation, provided insight on liquefaction analysis, and assisted in manuscript preparation. **Erfan Syamsuddin** (Dr., Associate Professor of Geophysics Department) led and supervised the study, provided expertise on seismic methods, and critically reviewed the manuscript.

All authors have read and agreed to the published version of the manuscript.